

UNIVERSITY OF BASEL

DEPARTMENT OF PHYSICS

MASTER THESIS

---

**Towards the Control of Spin-Orbit  
Interaction in GaAs/GaAlAs Quantum Dots**

---

*Author:*  
Philip Häner

*Supervisor:*  
Prof. Dr. Dominik Zumbühl  
*Co-Supervisor:*  
Dr. Liuqi Yu



July 1, 2016

UNIVERSITÄT BASEL

PHILOSOPHISCH-NATURWISSENSCHAFTLICHE FAKULTÄT

**Erklärung zur wissenschaftlichen Redlichkeit**

(beinhaltet Erklärung zu Plagiat und Betrug)

~~Bachelorarbeit~~ / Masterarbeit (nicht Zutreffendes bitte streichen)

Titel der Arbeit (Druckschrift):

Towards control of spin-orbit interaction  
in GaAs/AlGaAs quantum dots

Name, Vorname (Druckschrift): Häner, Philipp

Matrikelnummer: 09-065-676

Hiermit erkläre ich, dass mir bei der Abfassung dieser Arbeit nur die darin angegebene Hilfe zuteil wurde und dass ich sie nur mit den in der Arbeit angegebenen Hilfsmitteln verfasst habe.

Ich habe sämtliche verwendeten Quellen erwähnt und gemäss anerkannten wissenschaftlichen Regeln zitiert.

Diese Erklärung wird ergänzt durch eine separat abgeschlossene Vereinbarung bezüglich der Veröffentlichung oder öffentlichen Zugänglichkeit dieser Arbeit.

ja     nein

Ort, Datum: Münchenstein, 1.7.2016

Unterschrift: P. Häner

*Dieses Blatt ist in die Bachelor-, resp. Masterarbeit einzufügen.*



# Contents

<b>1. Introduction</b>	<b>1</b>
<b>2. Theory</b>	<b>4</b>
2.1. GaAs Quantum Well . . . . .	4
2.2. Spin-Orbit Interaction . . . . .	6
2.3. The Spin Qubit . . . . .	9
2.4. Electron Dipole Spin Resonance . . . . .	9
<b>3. Materials and Methods</b>	<b>11</b>
3.1. Wafer & Gate Design . . . . .	11
3.2. Experimental Setup . . . . .	12
<b>4. The Quantum Dot</b>	<b>14</b>
4.1. Transport Measurements . . . . .	17
4.2. Quantum Dot Characterization . . . . .	19
4.3. Charge State Measurements of the Quantum Dot . . . . .	20
<b>5. Conclusion</b>	<b>27</b>
<b>6. Outlook</b>	<b>28</b>
<b>7. Acknowledgements</b>	<b>29</b>
<b>Appendices</b>	<b>30</b>
<b>A. Gate Configurations</b>	<b>31</b>

# 1. Introduction

Conventional computation, as it is being done up to this day, use transistors as their basic unit of computation. A transistor can electrically be set to either 0 or 1 forming a bit. Many bits together are operated using gates to perform computational operations. Improving the computation power of transistor based computers is mainly based on downscaling transistors and thereby increasing the amount of transistors on a microprocessor. Improving conventional computers is thus limited by the advances made in the fabrication of transistors.

The time to perform a task with a conventional computer decreases linearly with the number of transistors (considering brute force method). In contrast, there are numerous problems with exponentially increasing complexity (e.g. factorization of large numbers). Solving these high complexity problems would require nearly infinite time even with continuously improving algorithms. The basic computational unit of the conventional computer is, and will always be, the bit.

As the size of a transistor is permanently decreased quantum phenomena drastically change properties of semiconductor structures in the nanometer regime. Quantum mechanics has to be taken into account to fabricate devices on the nanometer scale. Besides controlling these phenomena to fabricate better transistors for conventional computation, quantum mechanics by itself could be used to redefine the bit and do quantum computation. The basic unit of quantum computation is the qubit. The qubit is a fermionic two level system with basis states 0 and 1. The qubit, as it is defined by quantum mechanical states, is not necessarily in one or the other basis state but in a superposition of both of them. The most general basis state of a qubit is

$$|\Psi\rangle = \alpha |0\rangle + \beta |1\rangle. \quad (1.1)$$

where  $\alpha^2$  and  $\beta^2$  are the probabilities of the system to be in the corresponding state and  $\alpha^2 + \beta^2 = 1$ . The actual state is thus statistically distributed over the two basis states. A system containing multiple qubits can thus be in a large num-

ber of states with a given probability distribution. This offers more computational possibilities and would even allow to tackle the high complexity problems unable to be solved by conventional computers. Peter Wilson Shore was one of the first highlighting the potential of quantum computation by suggesting quantum algorithms to factorize numbers more efficiently [1]. The downside of using qubits, as they are defined by quantum mechanical states is, that they are very susceptible to noise. Noise can lead to errors in codes and corrupt the qubits. As for conventional computers errors can corrupt qubits and must be corrected to compute reliably. For a basic read on quantum error correction the reader is recommended to have a look at the dissertation of Daniel Gottesman [2]. Many theoretical proposals have suggested different kind of implementations of qubits, such as Rydberg atoms [3], diamond N-V centers [4], superconducting circuits [5] and electron spins [6]. The following electron spin based systems including carbon nanotubes [7], semiconducting nanowires [8] and gate-defined dots on semiconductor heterostructures [9] have been intensely studied. In lateral quantum dots the qubit is the spin  $\frac{1}{2}$  state of a spatially localized electron in a magnetic field. Heterostructures of a various semiconductors such as Gallium-Arsenide/Aluminium-Gallium-Arsenide (GaAs/AlGaAS) or Silicon/Silicon-Germanium (Si-SiGe) have been investigated. A major issue to allow quantum computation is the relaxation time  $T_1$ . The qubit couples to multiple energetic systems in its environment. Spin-orbit coupling, where an electrons magnetic moment couples to magnetic field induced by the electrons movement within an electric field, is one mechanism randomizing spins resulting in more rapid relaxation of the qubit.

In GaAs heterostructures two sources of internal electrical fields, namely the Dresselhaus field induced by bulk inversion asymmetry (BIA) and the Rashba field induced by structure inversion asymmetry (SIA) are observed. It has been shown that the spin-orbit field in GaAs heterostructures can be controlled by applying electrical fields. It has been theoretically predicted that it is possible to tune spin-orbit coupling into a regime, where an effect called persistent spin-helix leads to coherence times going towards infinity [10]. Knap et al. has shown that this system tunable into a regime electrons are more robust to spin independent scattering and prolonged coherence lengths lead to weak anti-localization effects [11].

The Quantum Coherence Lab of Prof. Dr. D. Zumbühl follows the predictions of Khaetskii et al. and Aleiner et al. and has developed a design which should allow to locally control spin-orbit interaction in quantum dots [12], [13]. The goal is furthermore to spatially displace single electrons within the intrinsic

spin-orbit fields at high frequency to perform Electron dipole spin resonance. In this thesis a GaAs/AlGaAs wafer specifically fabricated (Awschalom group, University of Santa Barbara, California) for the control of spin-orbit coupling and anti-localization measurements is investigated for the possibility of creating single electron quantum dots. Back- and top-gates (BG and TGs) are used to form quantum dots within a two dimensional electron gas(2DEG) formed in a GaAs/AlGaAs quantum well. A newer design using TGs to locally control spin-orbit interaction is being fabricated but no functioning devices have been found so far. The goal of this thesis was to show the potential of the wafer to efficiently form and characterize quantum dots. Characterization of the quantum dots showed, that we are capable of forming and measuring a quantum dot, but that the wafer has a very low mobility and there is a lot of disorder in the 2DEG. The device studied in this thesis therefore does not allow to perform spin-orbit interaction measurements on single electron spins. Even though this thesis does not show the most promising results for future measurements, it is very likely that higher mobility/less disorder and allow the formation of single electron quantum dots. In ongoing work the focus lays on devices which show a higher electron mobility in the 2DEG and the new TG-design is introduced.

## 2. Theory

In this section the properties of GaAs and specially GaAs quantum wells are introduced. It further will be shown, how we suggest to use intrinsic electric fields present in GaAs quantum wells to perform electron dipole spin resonance.

### 2.1. GaAs Quantum Well

GaAs is a III-IV compound semiconductor which forms a zinc-blende crystal. The band gap between valence and conduction band is 1.44 eV. By growing GaAs with a fraction of Gallium replaced with Aluminum ( $\text{Al}_x\text{Ga}_{1-x}\text{As}$ ) the band gap can be tuned within a range from 1.44 eV to 2 eV (for Al concentrations up to 30%). The exchange of lattice atoms has little influence on the crystal lattice introducing only a deviation of roughly 0.5%. An interface between GaAs and AlGaAs therefore has only little strain due to this small difference in lattice constants. The conduction

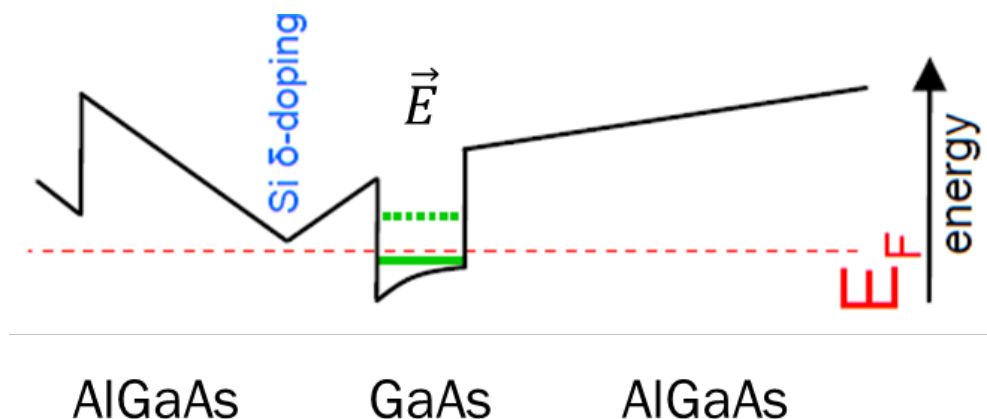


**Figure 2.1.:** a) Valence and conduction bands of AlGaAs (A) and GaAs (B) in contact with each other. The percentage of Al replacing Ga defines the increase in the band gap b) Energy bands in the same heterostructure as shown in a) with a doping introduced excess of charge carriers. Electrons migrate from A to B until the electrochemical is aligned. Band bending towards the heterostructure due to migrated electrons. [14]

band of a GaAs/AlGaAs quantum well is shown in figure 2.1. The band-gap

mismatch leads to the formation of the well in the sandwiched GaAs layer. A  $\delta$ -doping layer is grown in the AlGaAs phase introducing Si donor atoms and thereby additional charge carriers (n-doping). At room temperature the electrons have the energy to enter the quantum well. Reducing thermal energy towards  $T = 0K$  disallows electron to leave the quantum well. Electrostatic attraction draws the electrons towards the positively charge Si cores and the conduction band bends at the heterostructure as electrons accumulate and the electric field builds up. This is visualized by the slope introduced in the quantum well as the derivative of the band is the electric field  $E$ . The amount of dopant introduced in the  $\delta$ -doping layer is set to fill the quantum well with electrons and raise the Fermi level such that only the lowest sub-band is occupied. The electrons in this sub-band are restricted in two dimensions. This system is called two dimensional electron gas.

The density of states (DOS) for a two dimensional system is given by

$$D_{2D} = \frac{m^*}{2\pi\hbar^2}, \quad (2.1)$$

with the reduced electron mass  $m^* = 0.67 m_e$  for GaAs.

The density of states is constant and independent of the charge carrier density  $n = k_f^2/(2\pi)$  and the Fermi wave vector  $k_f$ . The charge carriers (the electrons) involved in transport behave in two dimensions like quasi-free particles with energy

$$E_f = \frac{\hbar^2 k_f^2}{2m^*}. \quad (2.2)$$

Only electrons with exactly the Fermi wave vector contribute to the transport in the 2DEG. Electrons with lower momentum cancel out each other's contribution to transport.

## 2.2. Spin-Orbit Interaction

The coupling of an electron's magnetic moment to its orbital motion is well known from electrons orbiting atomic nuclei. The coupling of the spin to its motion in an electric field is a relativistic effect. Electrons moving at high velocities  $\vec{v}$  within an electric field  $\vec{E}$  are experiencing a magnetic field  $\vec{B}_{SO}$ . The magnetic field is perpendicular to the direction of the electron movement and the electric field. The effective magnetic field is

$$\vec{B}_{SO} = -\frac{v}{c^2} \times \vec{E}. \quad (2.3)$$

Electrons within GaAs/AlGaAs heterostructures typically move at the Fermi velocity of  $195'000 \frac{m}{s}$  and are therefore influenced by relativistic effects. In AlGaAs/GaAs heterostructures there are two main sources known to be responsible for intrinsic electric fields, namely BIA and SIA. In bulk Si the crystal lattice is perfectly symmetric. GaAs in comparison forms a zinc-blende lattice where two superimposed FCC lattices, each consisting of either Gallium or Arsenide, form the unit cell. The asymmetric distribution of the different atoms leads to a permanent electric field. The Hamiltonian for the coupling of an electrons spin to the electric field originating from BIA is:

$$\mathcal{H}_{SO}^D = \gamma [\sigma_x k_x k_z^2 - \sigma_x k_x k_y^2 + \sigma_y k_y k_x^2 - \sigma_y k_y k_z^2 + \sigma_z k_z k_x^2 - \sigma_z k_z k_y^2] \quad (2.4)$$

In a 2DEG the electrons are highly confined along the z-axis, therefore the wave vector operator is replaceable by its expectation value  $k_z = \langle k_z \rangle = 0$  and  $k_z^2 = \langle k_z^2 \rangle \neq 0$ . Splitting the Hamiltonian into linear and cubic term leads to:

$$\mathcal{H}_{SO}^{D1} = \beta_1 (\sigma_x k_x - \sigma_y k_y) \quad (2.5)$$

$$\mathcal{H}_{SO}^{D3} = \gamma (\sigma_y k_y k_x^2 - \sigma_x k_x k_y^2) \quad (2.6)$$

which, using the relativistic approach from eq.2.3, leads to internal magnetic fields

$$B_{SO}^{D1} = \frac{2\beta_1}{g\mu_B} \begin{pmatrix} k_x \\ -k_y \end{pmatrix} \quad (2.7)$$

$$B_{SO}^{D3} = \frac{2\beta_3}{g\mu_B} \begin{pmatrix} -k_x k_y^2 \\ k_y k_x^2 \end{pmatrix} \quad (2.8)$$

SIA fields do not occur in the the bulk semiconductor but originate from structural asymmetry. The asymmetry responsible for the so-called Rashba field is the asymmetry in the quantum well introduced by the  $\delta$ -doping layer. In the experiments where spin-orbit fields are to be controlled Rashba spin-orbit coupling is desired and the well is designed asymmetrically on purpose. Rashba type electric fields therefore occur along the growth direction of the crystal (z-axis). The Hamiltonian for Rashba-type electric fields is

$$\mathcal{H}_{SO}^R = \alpha (\sigma_x k_y - \sigma_y k_x). \quad (2.9)$$

The Rashba Hamiltonian can be used to determine the magnetic field which is

$$B_{SO}^R = \frac{2\alpha}{g\mu_B} \begin{pmatrix} k_y \\ -k_x \end{pmatrix}. \quad (2.10)$$

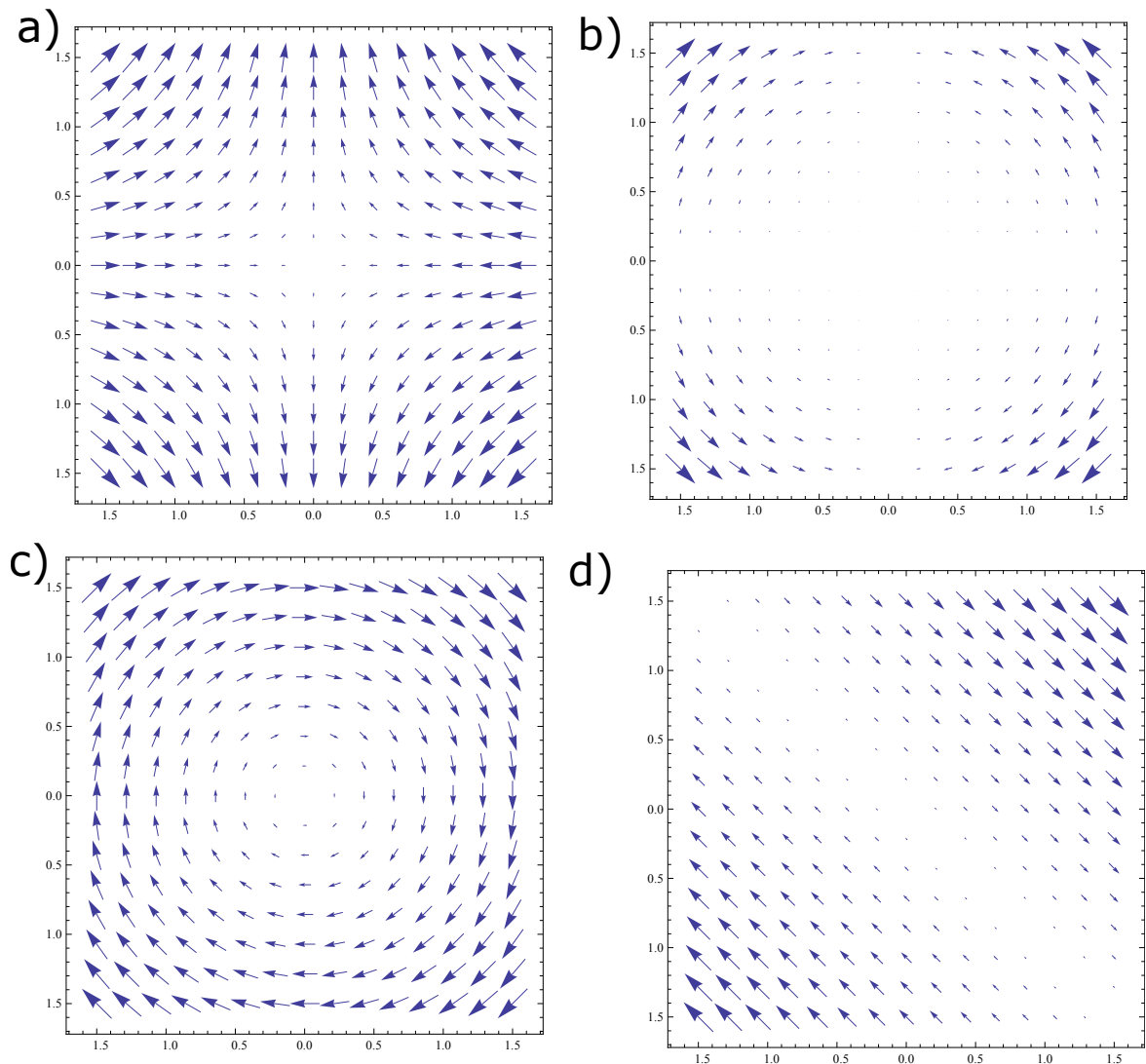


**Figure 2.2.:** Axis in all images: the x-axis is the  $k_x$  wave vector and the y-axis is the  $k_y$  wave vector. Spin-orbit fields are shown as blue arrow. The longer an arrow, the bigger is the spin-orbit field. a) linear Dresselhaus field b) cubic Dresselhaus field c) linear Rashba term d) Spin-orbit field in the regime where  $\alpha = \beta$ . The field is unidirectional for any  $k$ .

As both sources for spin-orbit coupling have been determined the spin-orbit coupling Hamiltonian, excluding the cubic Dresselhaus terms because they are dominated by the linear terms, is

$$\mathcal{H}_{SO} = \alpha (\sigma_x k_y - \sigma_y k_x) + \beta (\sigma_x k_x - \sigma_y k_y). \quad (2.11)$$

As the Rashba field originates from manufactured structures in the crystal and points along the growth direction, the growth direction itself can be chosen to be 001 and thus leads to the Rashba and Dresselhaus fields pointing in the same direction. The Rashba field derives from the electric field between  $\delta$ -doping layer

and the 2DEG and is therefore tunable by applying an external electric field. It is possible to tune it into a regime where the Dresselhaus and the Rashba coefficients are similar. These intrinsic fields are to be used to perform EDSR on spin-qubits discussed in depth in the following section.

## 2.3. The Spin Qubit

An electron has a magnetic moment called spin. Without a magnetic field the spin orientation is randomized and the electron is equally likely to be in the state  $|\uparrow\rangle$  or  $|\downarrow\rangle$  and the states are energetically degenerate. The application of a magnetic field  $\vec{B}$  provides a polarization axis and lifts the degeneracy of the spin states. This effect is called the Zeeman effect and the energy by which the degeneracy is lifted is given by the Zeeman-energy

$$E_{Zeeman} = g\mu_B B = \hbar\omega_L, \quad (2.12)$$

where  $g$  is the Land-factor,  $\mu_B$  is the Bohr-magneton,  $B$  is the magnetic field strength and  $\omega_L$  is the Larmor frequency. As the spin orients itself along the magnetic field axis, inertia leads to Larmor precession around the polarization axis at the Larmor frequency  $\omega_L$ . This system is called the spin qubit.

## 2.4. Electron Dipole Spin Resonance

Manipulation of the qubit state is necessary to perform computational operation. To manipulate the spin qubit the magnetic moment is to be addressed. To manipulate the spin of an electron a magnetic field oscillating at the Larmor frequency is needed. The resonant driving of the transition and the energy inserted into the system can't be translated into higher Larmor frequency, as it is fixed by the Zeeman-energy. Instead it is translated in the change of angular momentum and the qubit state rotates on the surface of the Bloch sphere as shown in figure 2.3. The frequency at which the rotation on the Bloch sphere occurs is given by the Rabi frequency

$$\Omega = g\mu_B B_{\perp}/\hbar, \quad (2.13)$$

where  $B_{\perp}$  is the amplitude of an oscillating magnetic  $B_{x,y} = B_{\perp}(\cos(\omega t) + \sin(\omega t))$  field perpendicular to an external magnetic field  $B$  acting as polarization axis and defining the Zeeman-energy. As the rotation depends on the amplitude of the oscillating field and time, the duration of the resonant drive defines the rotation pulse.

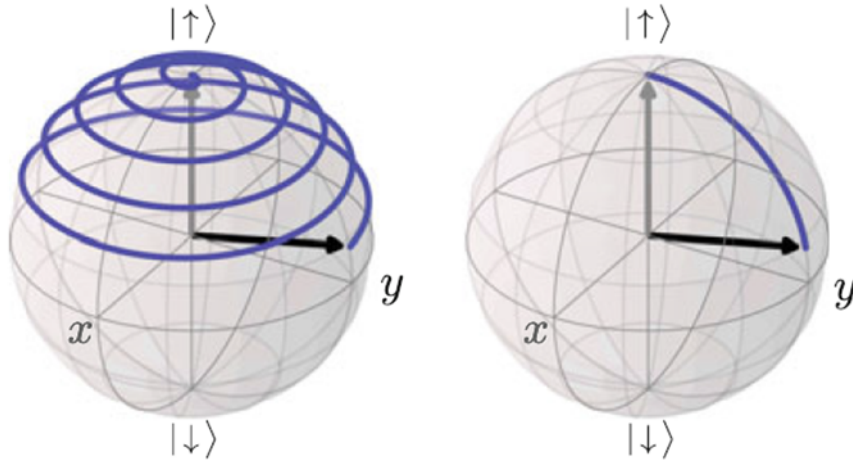


**Figure 2.3.:** Bloch sphere representation of electron spin in magnetic field. The blue line shows the spin precession around the polarization axis. Resonant drive at the Larmor frequency leads to a spin-flip rotation.

It is difficult to apply oscillating magnetic fields at high frequencies and externally applied magnetic fields are therefore no valid options to drive the spin-flip transition. We have shown in chapter "Spin-Orbit Interaction" how electric fields, for fast electrons, translate into magnetic fields. And the coupling of such an electric field to the spin of an electron is called electron dipole spin resonance.

Exemplary magnetic field induced by spin-orbit interaction within GaAs quantum wells are shown in figure 2.2. We want to do EDSR by spatially displacing electrons within the intrinsic spin-orbit fields at the Larmor frequency. To do so we need a wafer allowing control of spin-orbit interaction and a means to isolate single electrons and spatially displace them at high frequencies.

# 3. Materials and Methods

The theory needed to perform EDSR on electrons has brought up some basic requirements which need to be fulfilled. In this section the means to characterize a quantum dot formed in a wafer grown to allow control of spin-orbit interaction are introduced.

## 3.1. Wafer & Gate Design

The growth profile of the GaAs Wafer investigated in this thesis is shown in figure 3.1a. The wafer was grown by Shawn Mack and David Awschalom in Santa Barbara. The wafer is grown on an  $n^+$  doped GaAs substrate which acts as the BG. The quantum well is positioned 1210  $nm$  above the BG and 75  $nm$  below the surface and is formed within a 9.3  $nm$  GaAs layer between layers of AlGaAs. The Silicon  $\delta$ -doping layer for asymmetric doping is positioned 12  $nm$  above the quantum well. The 600  $nm$  GaAs layer grown at low temperature (GaAs LT) has a high resistivity and prevents leaks between BG and quantum well [15]. The major flat corresponds to the 100 and the minor flat to the 010 crystalline directions. The 001 crystalline direction is set along the growth axis leading to the Rashba and Dresselhaus electric field pointing along the growth direction. The wafer was fabricated to at  $T = 0$  and no electric fields applied have Rashba field strength equal to the Dresselhaus field strength  $\alpha \approx \beta$  (doping amount, distance to the quantum well, size of the quantum well). The 2DEG has an electron density of  $n = 4.610^{11} cm^{-2}$  which leads to electrons having a Fermi wavelength  $\lambda_F \approx 37 nm$ . The mobility of the wafer is  $\mu = 69'000 cm^2/Vs$ , which is low for 2DEGs.

Figure 3.1b shows the top view of the wafer and the position which was cleaved and used for the device fabrication. The values for electron density and mobility given before are maximum values for the whole wafer. The effective values are most likely be lower.

Ohmic contacts to the 2DEG are fabricated using UV-photolithography and Annealing procedures. Au/Ge Top-gates are fabricated using e-beam-photolithography

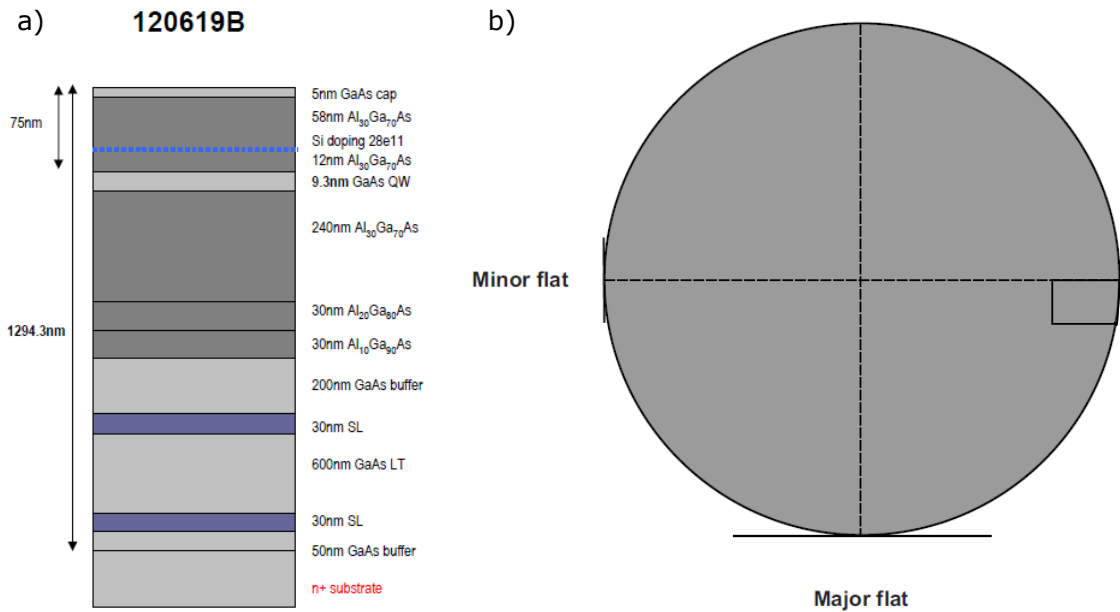


**Figure 3.1.:** a) Growth profile of the GaAs wafer. The 2DEG is positioned 75 nm below the surface. It is a double heterostructure with GaAs sandwiched between AlGaAs layers. A 600 nm GaAs layer grown at low temperature acts as a leakage protection between the 2DEG and the BG at the very bottom of the wafer. b) Top view on Wafer. The black square shows the part of the wafer which was cleaved and used for the device fabrication.

and thermal evaporation. The TG configuration is shown in figure 3.2. The gates have a width of  $\sim 50\text{nm}$ . The design is taken from S. Amasha and modified to reduce the distances between gates [16]. The main quantum dot gates Nose, Left Wall (LW), Left Plunger (LP), Middle Plunger (MP), Right Plunger (RP) and Right Wall (RW) are used to for a main quantum dot. The gates Left Splitter (LS) and Right Splitter (RS) are used to divide the 2DEG underneath into main dot transport and sensing regions which is necessary to bias main dot/sensor individually. The gates Top Sensor (TS1/2), Middle Sensor (MS1/2) and Lower Sensor (LS1/2) are used to for sensors to measure the main dot.

## 3.2. Experimental Setup

To measure electronic transport through a 2DEG and form a quantum dot a low temperature setup and an electronic setup is required. The sample is mounted on a sample stage in a dilution refrigerator (MCK50). The temperature in the mixing chamber of the dilution refrigerator reaches  $\sim 30\text{ mK}$ . It is known from similar samples, that the electron temperature in the sample for the shown mixing chamber temperature is  $\sim 100\text{ mK}$ . A set of two Low Noise High Sensitivity

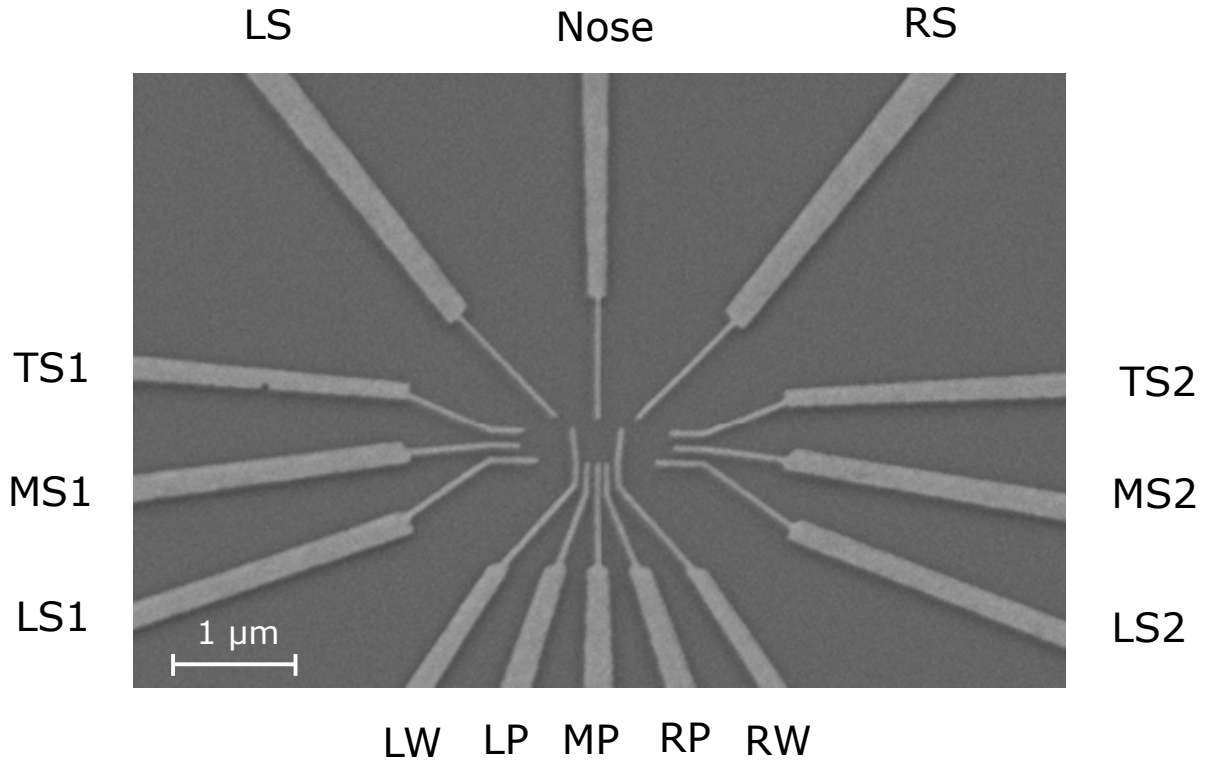


**Figure 3.2.:** Top-Gate design used in this thesis. Main dot gates: Nose, LW, RW, LP, MP, RP. Splitters: LS and RS. Sensor gates: TS1/2, MS1/2 and LS1/2

(LNHS) Digital Analog Converters (DAC) is used to apply voltages. The two DACs are used to apply negative voltages to Back- and Top-gates and apply voltage biases to the 2DEG. Sensitivity of the applied bias is increased by putting a 1 : 111 voltage divider in series with the 2DEG. A  $10M\Omega$  resistor is put in series to have stable currents through the 2DEG. The current through the 2DEG is drained and multiplied by an IV-converter and digitalized using Digital MultiMeters (DMMs).

## 4. The Quantum Dot

Having shown how electrons are restricted in two dimensions within a GaAs/AlGaAs quantum well, the x-y plane can be further restricted to form an actual quasi zero-dimensional quantum dot.

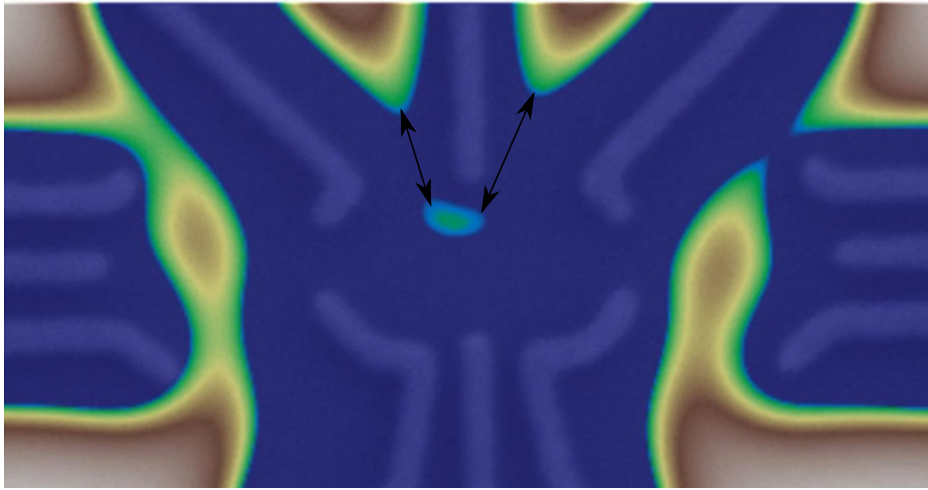


**Figure 4.1.:** Electron density simulation using SETE [17]. Electric fields deplete the 2DEG underneath (blue). Island of low electron density in the middle of the gates is the quantum dot (green). Black arrows are the tunnel couplings to the reservoirs. Image taken from [18].

Negative voltages are applied to top-gates to form a quantum dot. The electric field reduce the electron density  $n$  within the 2DEG. A simulation of the electron density in the 2DEG for a different gate arrangement is shown in figure 4.1. The color in the images represents decreasing electron density from brown (high) to green to blue (zero) as a function of gate voltages. The image shows three isolated and semi isolated regions of high electron density. As voltages on the gates are more negative, channels through the 2DEG are forming. The gate voltages can be set to form a quantum dot which is still connected to the rest of the 2DEG (reservoirs). The reservoirs are set to fixed potentials. On the left side of the simulation a circular region of high electron density, which is still connected to the reservoirs is shown (open quantum dot). In the middle position a fully isolated island of heightened electron density appears (closed quantum dot).

The potential containing electrons in the quantum dot is complex and difficult to describe mathematically. The potential can be approximated to be harmonic if we assume the shape of the quantum dot to be symmetric in x and y. The energy levels of the quantum harmonic oscillator are

$$E_n = \hbar\omega \left( n + \frac{1}{2} \right) \quad (4.1)$$

The energy level spacing is given by

$$\Delta = \hbar\omega \quad (4.2)$$

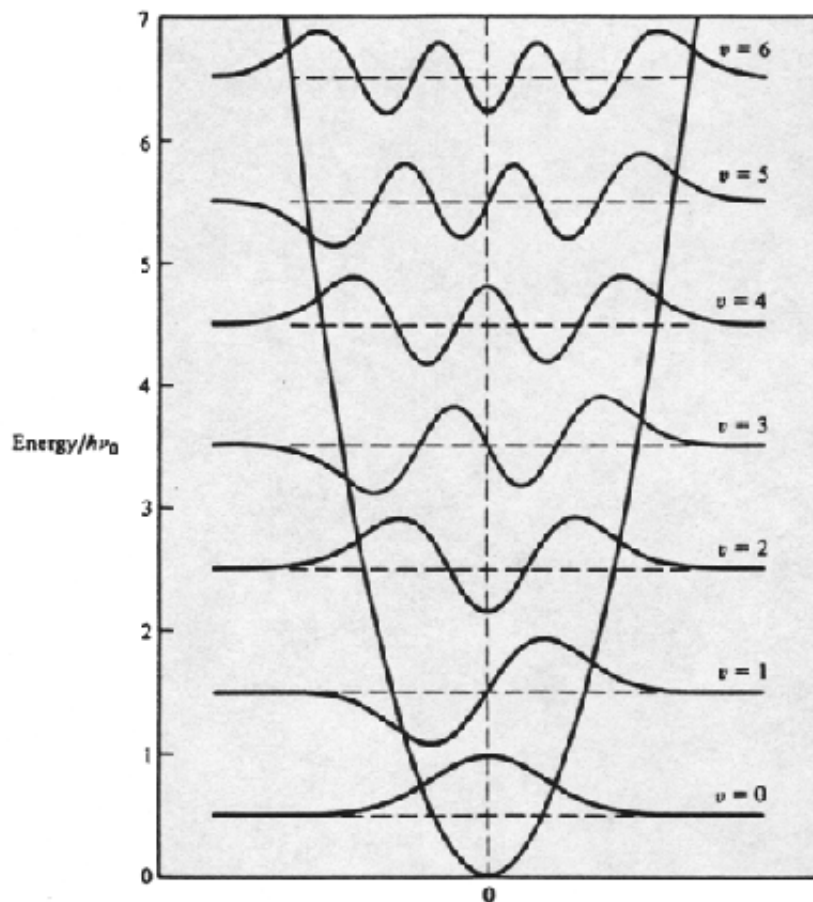


**Figure 4.2.:** Harmonic potential and the wave functions with quantized energy levels. [19].

The harmonic potential and its quantized orbital energy levels are shown in figure 4.2. For non-interacting electrons orbitals are filled until all orbitals of lower energy than the chemical potential of the 2DEG are filled. Starting from the

ground energy level each level holds 2, 6, 10, 14 electrons and so on. Electrons do repel each other and therefore it takes energy to overcome the repulsion and add another electron. This energy is called charging energy  $E_C$ . The charging energy depends on the number of electrons in the potential and the orbital it is filling, as orbitals have different spatial probability distributions. The energy needed to add an electron to the quantum dot is thereby given by

$$E_{add} = E_C + \Delta, \quad (4.3)$$

where  $\Delta$  is only nonzero when an electron enters an orbital on the next higher energy level. The energy level setting in the quantum dot depends on the width of the harmonic potential with  $E \propto \frac{1}{L^2}$ . As voltages on gates forming the quantum dot get more negative, the width of the quantum well decreases and the levels of the quantum shift upwards. This effect is called plunging and can be used to tune the quantum dot energy levels. The same absolute change in gate voltage on two different gates normally induces different shifts of the quantum dot energy levels. The corresponding relationship is given by the following equation

$$V_{Dot} = \alpha \cdot V_{Gate}, \quad (4.4)$$

where  $V_{Dot}$  is the change in energy in the dot (in eV),  $\alpha$  is the lever-arm for the gate of interest and  $V_{Gate}$  is the difference in voltage applied to the gate.

Figure 4.3 shows the chemical potential (grey) in relation to the quantum dot energy levels. In figure 4.3,a the quantum dot is filled with one electron. It takes only the charging energy to add the second electron. Electrons tunnel at frequencies  $\Gamma_S$  and  $\Gamma_S$  between quantum dot and reservoir as the level of the second electron aligns with the chemical potentials of the reservoirs. Between two quantum dot levels tunnelling is not allowed due to Coulomb repulsion and the dot is in Coulomb blockade. Lowering the dot energy levels and dis-aligning it by more positive gate voltages results in the quantum dot containing two electrons. With the addition of the second electron the orbital is full. Addition of the third electron opens a new orbital and does therefore take the orbital energy plus the charging energy.

Applying a DC-bias over the quantum dot opens up a bias window between the source and the drain chemical potential. Electrons will tunnel from the source

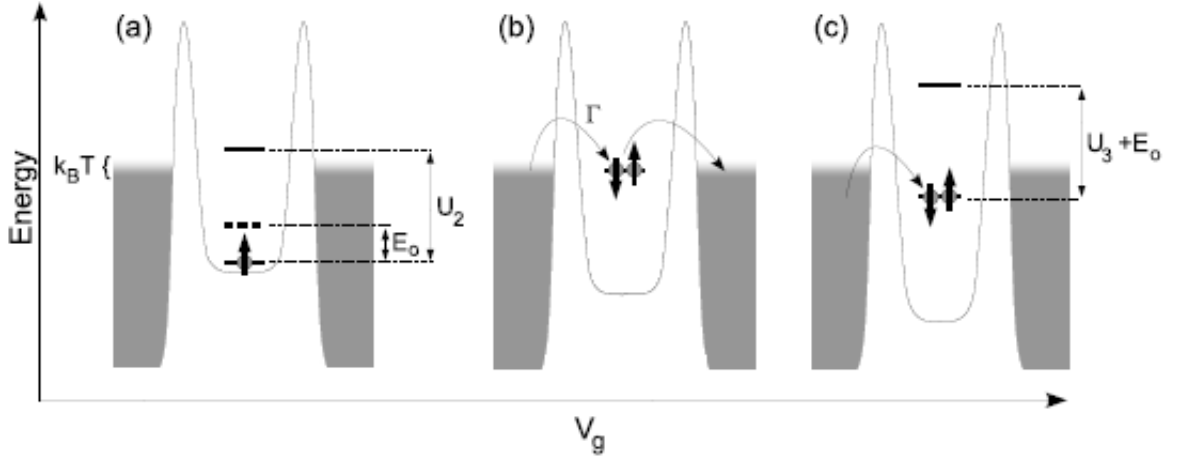


**Figure 4.3.:** The energy diagrams show the reservoir energy level with the Fermi level broadened by  $k_bT$ . The tunnelling frequency through the tunnel barriers is marked with  $\Gamma$ . a) Dot energy levels of singly occupied ground level. The dots orbital energy level for the second electron is marked with  $E_0 \equiv \Delta$ . The addition energy for the second electron is marked with  $U_2 \equiv E_C$ . b) Gate voltages lower the second dot level which aligns with the Fermi level and allows electrons to tunnel on and off the dot. c) Further decrease in gate voltage forbids the electron occupying the dot which leads to a dot filled with two electrons [16]

reservoir to the quantum dot and then to the drain reservoir whenever a quantum dot level is within the bias window. The current through the quantum dot is given by

$$I = e\Gamma, \quad (4.5)$$

where  $\Gamma$  is the lower tunnelling frequency amongst  $\Gamma_S$  and  $\Gamma_D$  and  $e$  is the electron charge.

## 4.1. Transport Measurements

The global charge carrier density within the 2DEG is manipulated by applying a negative voltage to the BG. The reduced charge carrier density in the 2DEG allows the voltage on the TG to be less negative to fully deplete the 2DEG. Without the negative BG voltage the TGs leak before fully depleting the 2DEG. It is not yet understood why the BG voltage is needed to prevent the leak. Applying voltages to any set of two TGs allows to form a quantum point contact (QPC) in between and to fully pinch-off the conductance through the channel. An exemplary pinch

curve is shown in figure 4.4. Voltages are applied to the Nose and RW closing the width of the conducting channel through the 2DEG. The conductance trace shows three different slopes. The first, steepest slope ranges from 0 mV to -250 mV. In this range the electric field of the gates depletes the 2DEG underneath. In the second region, from -350 mV to -1000 mV, the channel in the 2DEG narrows with more negative gate voltages and a quantum point contact is formed. In this wafer we know the electron density in the 2DEG and therefore calculate the Fermi wavelength  $\lambda_F = \sqrt{2\pi n} \approx 37 \text{ nm}$ . This value for the Fermi wavelength is the lower limit calculated for no applied BG voltage. In the experiments presented here  $\lambda_F > 37 \text{ nm}$ . Normally conductance plateaus for channel widths that are multiples of  $\lambda_F$  should be detected. Above -1000 mV and closer to the pinch, peaks of conductance similar to the Coulomb peaks found in quantum dots occur. The conductance is 0 when the size of the channel becomes smaller than  $\lambda_F$ . The wafer is known to have a low mobility and therefore a lot of disorder. We expect the Coulomb peak like features to derive from disorder potential coming from the doping layer or lattice defects. Disorder potentials may form barriers similar to the ones we form with the gate applied voltages. It is even possible that the disorder potential narrows the channel we form to begin with. As the channel width is reduced to less than  $\lambda_F = 37 \text{ nm}$  there is no conductance through the channel. The channel can be closed by either the potentials applied by the gates or a combination of gate potentials and disorder potentials.

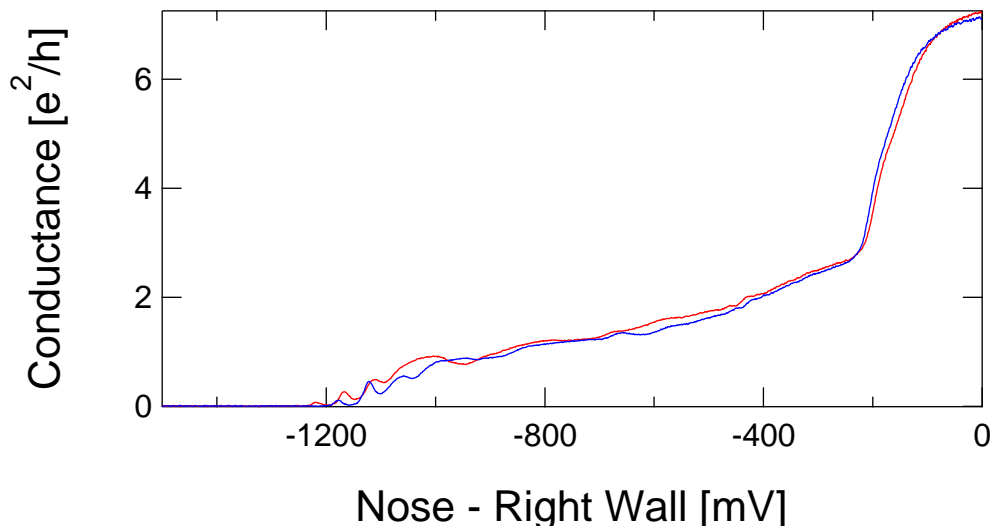


**Figure 4.4.:** Pinch-off curve of gates nose against RW. From 0 – (-250) mV the 2DEG underneath the gates is depleted. From 250 – (-1200)mV the channel is continuously narrowed until it is fully pinched. Irregularities in pinch-off behavior are especially apparent right before pinch-off.

The pinch-off voltages between the main dot gates are shown in figure 4.5. Pinch-off values between Nose-RW ( $-1200\text{ mV}$ ) and Nose-LW ( $-1260\text{ mV}$ ) have minor differences. The RW is thus shorter than the LW. Comparison of the LS-LW ( $1000\text{ mV}$ ) and the RS-RW ( $-1940\text{ mV}$ ) pinch-off leads to the conclusion that the LS is shorter than the RS. The difference in pinch-off voltage is  $\sim 5\%$  and barely influence the characterization measurements.

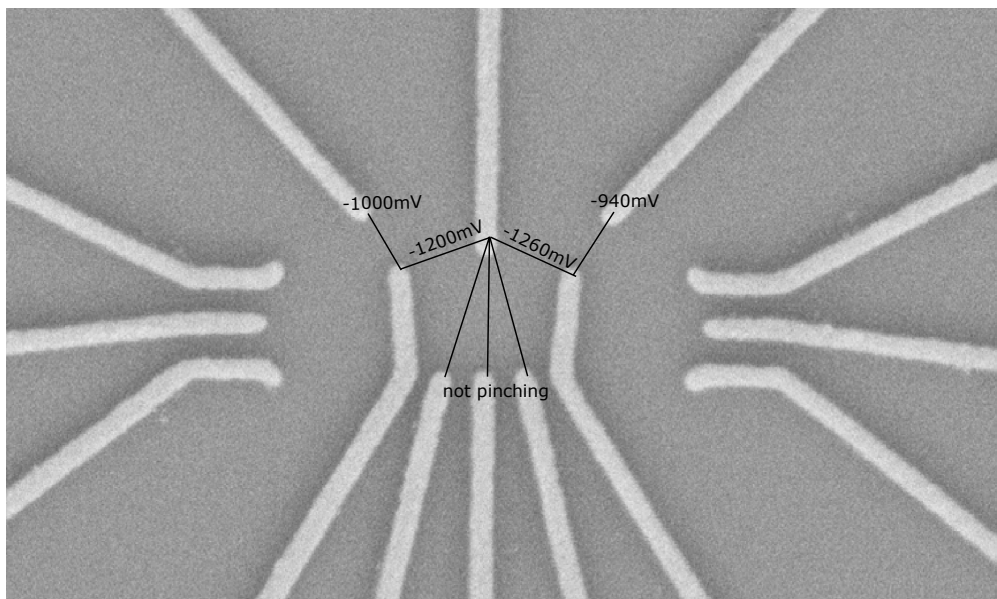


**Figure 4.5.:** Topgate arrangement on surface of the device. Drawn in black are the pinch-off Voltages between all main dot gates. Only minor differences in pinch-off voltages suggest a rather symmetrically fabricated device.

## 4.2. Quantum Dot Characterization

Gates Nose, RW, LW, LP, MP and RP are used to deplete the 2DEG and form a quantum dot. Figure 4.6 a shows the conductance through the dot in dependence of the left and right wall voltage; all other main dot gates are at fixed voltages. Gate voltage ranges are  $-600\text{ mV} - -1500\text{ mV}$ . The image shows the conductance through the dot as a function of the gate voltages. For low gate voltages on RW and LW ( $-600\text{ mV}$ ) areas of high conductance with hardly detectable lines on top of it are detected. The conductance channel width has not reached  $\lambda_F$  and conductance through the dot does not only depend on quantum dot level aligning but also on classical conductance through the channels formed. Figure 4.6 b shows a cut along RW through the data shown in a. The graph shows Coulomb peaks corresponding to the entering of a quantum dot energy level into the bias window.

For less negative RW voltage ( $-600\text{ mV}$ ) the conductance does not go to zero and the quantum dot is open. As voltages get more negative the conductance through the dot in between peaks goes to zero and the quantum dot is in Coulomb blockade. Each line visible in the 2D plot therefore corresponds to a transition of the quantum dot from being occupied with  $N$  electrons to  $N-1$  or  $N+1$  respectively. The Coulomb peaks are separated by a voltage of  $\sim 15\text{ mV}$  applied to the RW and  $\sim 20\text{ mV}$  applied to the LW. If the lever-arm is known Coulomb peak spacing in gate voltages can be translated into the actual addition energy using formula 4.4. In this thesis the no lever-arms were measured. The measurement nonetheless allows to make a relative statement about the lever-arms of gates RW and LW. The voltage difference between two Coulomb peaks is smaller for the RW than for the LW and the lever-arm of the RW is therefore larger. The quantum dot is therefore located closer to the RW .

In addition to the quantum dot features presented, some irregular features are found. The data shows an abrupt loss of conductance at  $\sim -1100\text{ mV}$  RW voltage and  $\sim -1200\text{ mV}$  LW voltage followed by small regions with conductance. We account this behavior as the one detected in the pinch of curve to quantum dots formed with the disorder potential. More precisely to a quantum formed very close to the channels pinched by the Nose and the LW/RW. If the disorder dot is in Coulomb blockade the conductance will be zero even if a main quantum dot energy level is in the bias window. The gate voltage area within which the disorder dot features appear corresponds well with the Coulomb peak features found in the pinch-off curves which supports that argument. The wafer disorder disturbs the measurement strongly and does not bring up conclusive data state of the quantum dot.

### 4.3. Charge State Measurements of the Quantum Dot

Measuring transport through a quantum dot has its limitations, as the coupling to the reservoir decreases with more negative gate voltages, the height and the width of the potential barrier increases. The tunnelling frequency into the dot gets lower and the current isn't measurable anymore. The loss of signal in transport measurements can be bypassed by accessing the quantum dots charge state. Changing voltage on gates forming the main quantum dot fills or empties the

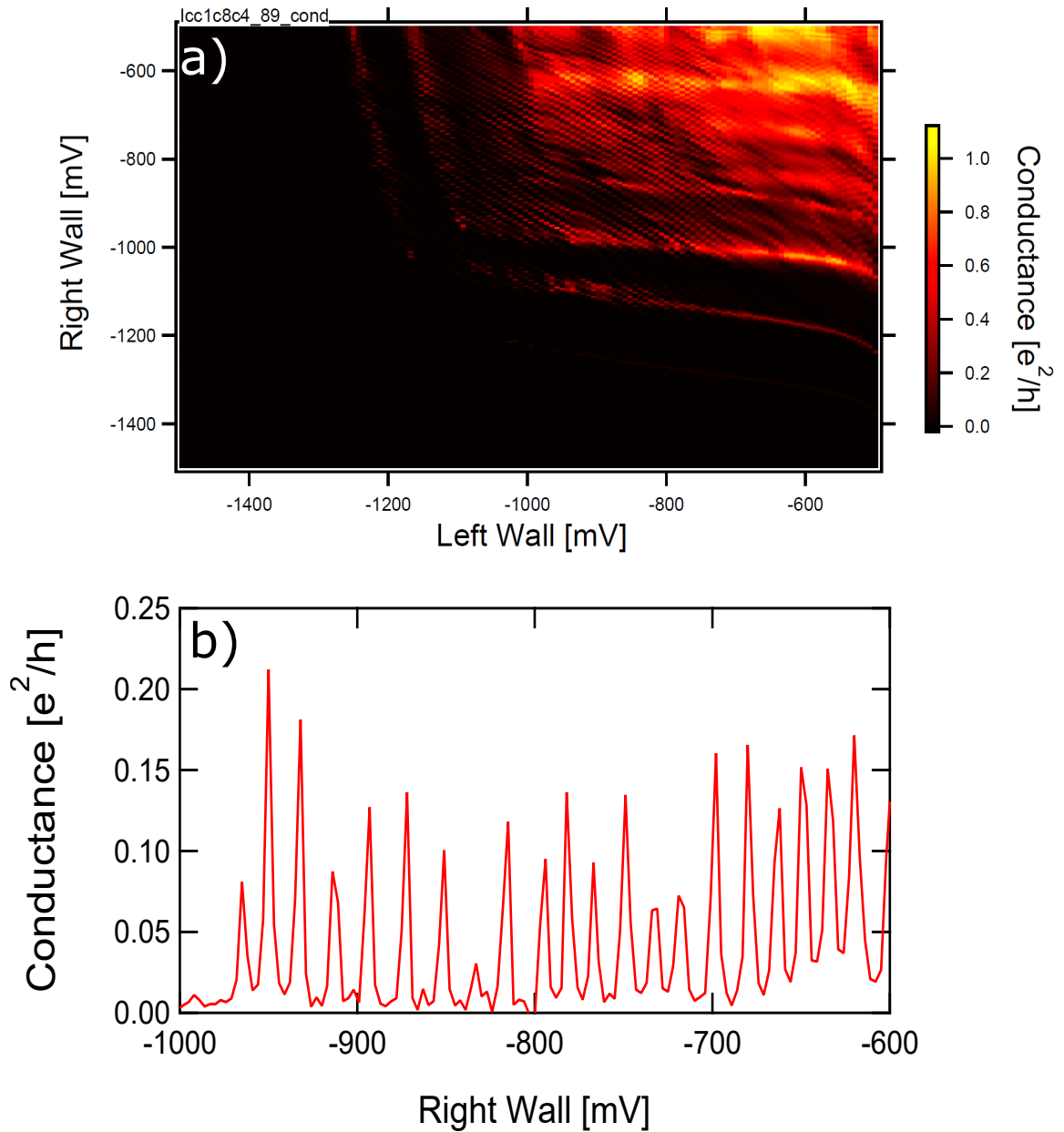


**Figure 4.6.:** a) Two dimensional plot of conductivity through a quantum dot. Transport through the quantum dot is measured as the left wall (LW) is run against the right wall (RW) of the main dot. The green line is a cut along the y-axis and is shown in b). Gate configuration shown in A.1. b) Conductivity as a function of right wall voltage. Coulomb peaks with a level spacing of  $\sim 20$  mV are shown.

quantum dot electron by electron. Each electron added/taken from the quantum dot raises/lowers the charge state of the quantum dot by one electron charge. The charge state of the quantum dot is accessed by placing a quantum object, such as a QPC or another quantum dot in close proximity to the main quantum dot. The change in charge state leads to a stronger electric field emitted, plunging the sensor and therefore changing the conductance through the sensor.

We do not need to measure the conductance over the main quantum dot, as we are interested in it's the charge state. Bias across the main quantum dot is set to zero because tunnelling events happen as quantum dot levels align with the chemical potential. The 2DEG underneath gate RS is depleted to isolate the left sensor side and individually bias the sensor. The main quantum dot gates are at fixed voltages, where the LW is set to the smallest value ( $-800\text{ mV}$ ) required to form a closed dot and maximize coupling to the sensor. The sensor side is biased and negative voltage is applied to the gate TS1. The conductance as a function of the voltage on gate TS1 is shown in figure 4.7. The measurement shows Coulomb peaks where conductance in between is non-zero suggesting that, similar to the measurement for the formation of a QPC, an open quantum dot is formed somewhere between the gates LW, LS, TS1 and random disorder. The dips in conductance at  $-1010\text{ mV}$  and  $-900\text{ mV}$  are first signs of switching noise/telegraph noise being introduced by going more negative on all gates. Switching noise is going to be discussed in more detail later in this chapter. Many Sensor gate arrangements on both sides of the main quantum dot have been studied.

The change in conductance is maximized when the sensor gate voltage is set to a value where the slope of the conductance measurement is at its maximum. The sensor gate was therefore set to be on the flank of the peak with steepest slope ( $\sim -1000\text{ mV}$ ). Every gate used to form the main quantum dot act also as a plunger on the sensor quantum dot. All gates with changing voltage during a measurement are going to be linearly corrected. This allowed to get charge sensing signal over a large range of gate voltages.

Figure 4.8 a shows transport through the sensor as a function of the voltages on the Nose and RW. Maximum conductance values are around  $25\ e^2/h$  which corresponds to the conductance peak chosen as sensor. Main quantum dot electron transitions can be observed as parallel lines. A cut along the nose (green line) is shown in figure 4.8 b. The graph shows the conductance as a function of the Nose voltage. The plot shows jumps in conduction of  $\sim 3.5 * 10^{-3}\ e^2/h$  corresponding to a change of  $\sim 4\%$ . The coupling between the main quantum dot and the sensor dot is relatively small. On other devices measured in Zumbühl group charge sensing signals  $> 50\%$ . We do not understand why the coupling is this weak in the sample as the gate configuration is specifically chosen to maximize the coupling. The corrections applied to the sensor gate can be seen to not perfectly correct the drift of the sensing position but allows to detect the main quantum dot charge state over a range of  $400\text{ mV}$ . The derivative with respect to the nose is taken and shown

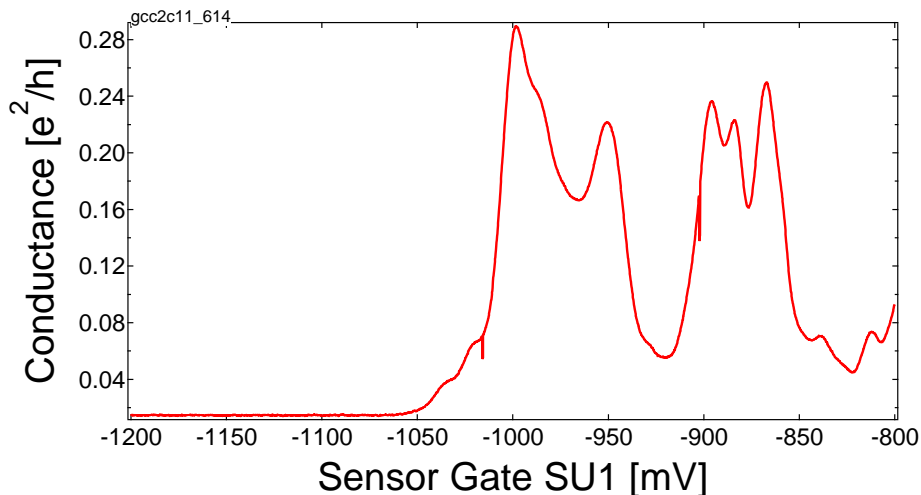


**Figure 4.7.:** Formation of a mixture between a QPC and a sensor dot using gate SU1. No proper coulomb peaks and no proper conductance plateaus are found. Gate configuration shown in A.2.

in figure 4.9 a. The differentiated graph reveals multiple electron transitions not visible in the not differentiated graph. There are two dots which do couple strongly to the sensor the slopes of which are highlighted in green and blue in figure 4.9 b. Besides their strong coupling to the sensor there are anti-crossings to be found where the electron transitions intersect each other. At such an anti-crossing the sum of electrons in both dots stays the same, but an electron tunnels from one quantum dot to the other. Electron transition are found for the whole measured gate range for the main quantum dot (blue). The second quantum dot (green) has no transitions after the highlighted one and the last electron was therefore pushed out of the quantum dot. The lever-arm of both gates on the second quantum dot is much smaller than the lever-arm of the gates on the main quantum dot. The Main quantum dot is therefore likely to be close to the left wall. The second quantum dot is most likely due to disorder formed in a more central position between all main quantum dot gates.

In addition to the two strong coupling quantum dots multiple electron transitions with different slopes are found. Multiple additional disorder dots must therefore be introduced in greater distance to the charge sensor (light blue). These quantum dots are most likely the ones disturbing the transport measurement and in the region between the gates Nose and LW/RW. Due to the difference in coupling to the sensor and the assumed larger distance, tunnelling interaction between the main quantum dot and the addition dots is not observable. It is very likely that the strong coupling quantum dots have tunnelling coupling to the left reservoir

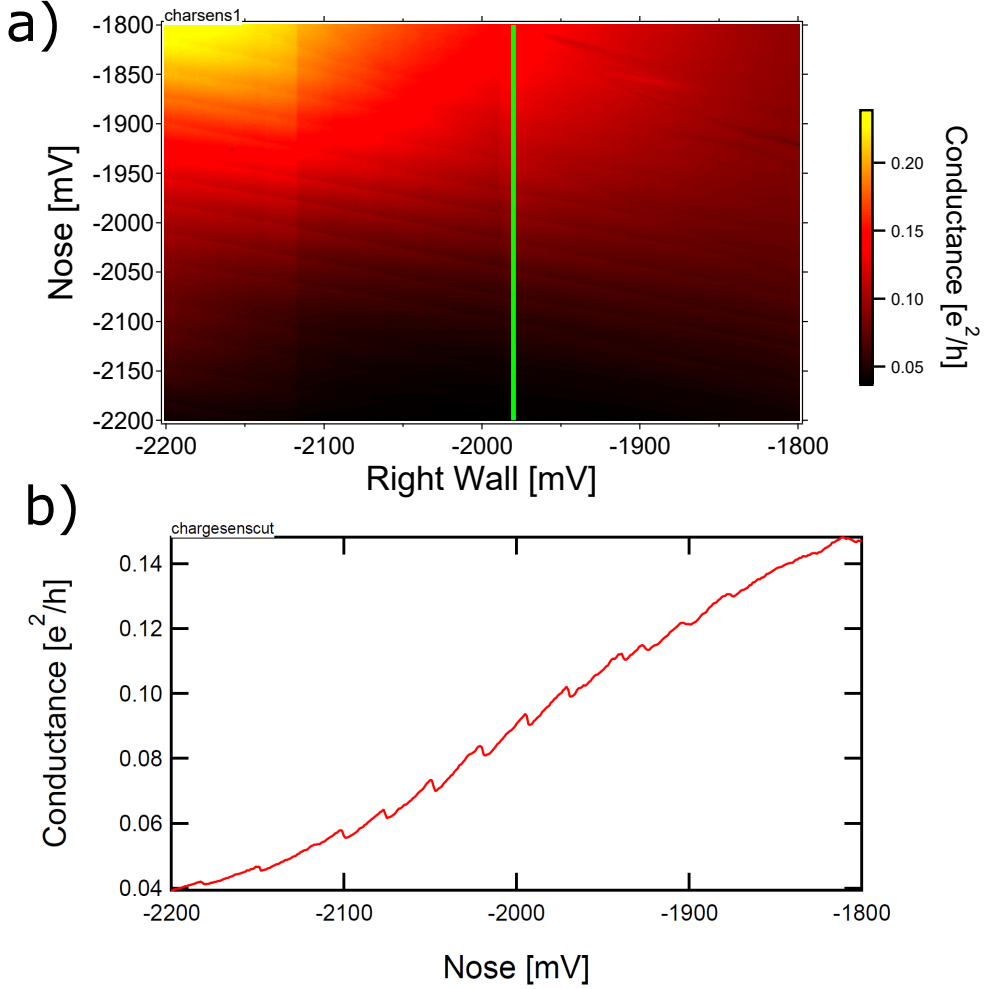


**Figure 4.8.:** a) Transport through sensor while gates NOSE and RW are run against each other. Parallel lines which correspond to a change in the charge state of the main quantum dot are visible. Green line is a cut along the NOSE and is shown in b). Gate configuration shown in A.3. b) Cut along the green line shown in a). Sharp conductance ( $\sim 4\%$ ) jumps corresponding to a change of the main quantum dot charge state.

and the weak coupling ones to the right reservoir.

Further charge sensing measurements and sensor optimizations are performed to search for the last electron transition. Figure 4.10 shows the differential of the conductance in respect to the Nose as a function of Nose and RW voltage. In this measurement the plunger gates LP, MP, RP are set at more negative voltages and the range on RW is going more negative as well. The measurement shows only electron transitions which suggests that the disorder dots are empty. Electron transitions are found and have a spacing of  $\sim 50$  mV on the Nose. The range on the measurement, an additional 75 mV after the last found transition does not allow to make statement about the electron number in the dot. A

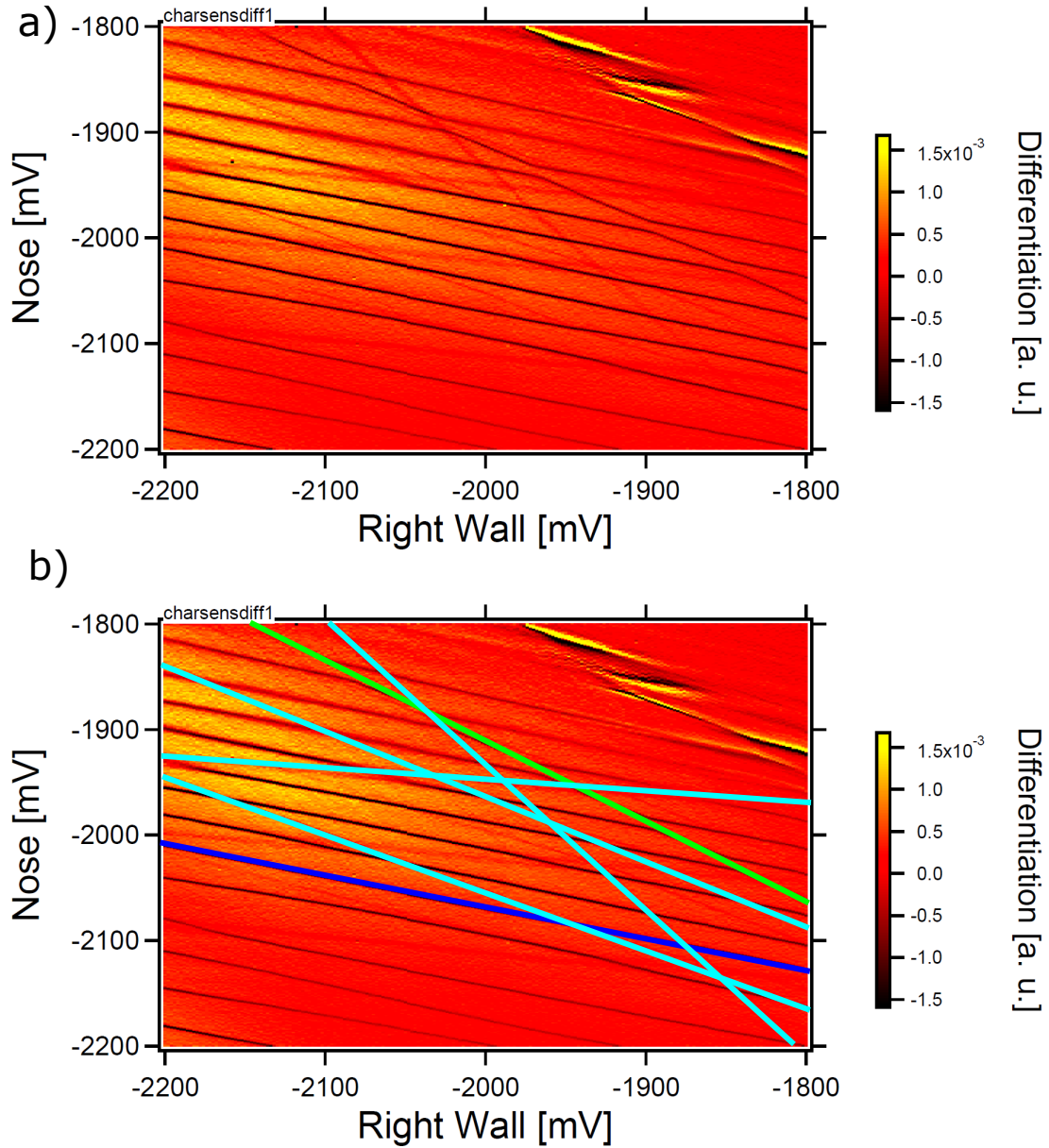


**Figure 4.9.:** a) Conductance plot derivative with respect to the Nose gate and as a function of Nose and Right Wall voltage. b) Colored lines do differentiate between main quantum dot (blue), second quantum dot (green) and additional weak coupling quantum dots.

conductance measurement with more negative gate voltage on LP, MP and RP ( $-2100 \text{ mV}$ ) is shown in figure 4.11. The measurement is disturbed by short-lived switching/telegraph noise. The origin of the the switching noise is unclear, but it is supposed to be coming from electrons in the spacer layer between the quantum well and the  $\delta$ -doping layer. Such electrons momentarily are released of their position and the proximity to the 2DEG and the coupling to the sensor leads to strong changes in conductance. Setting the plunger gates to ( $-2100 \text{ mV}$ ) will

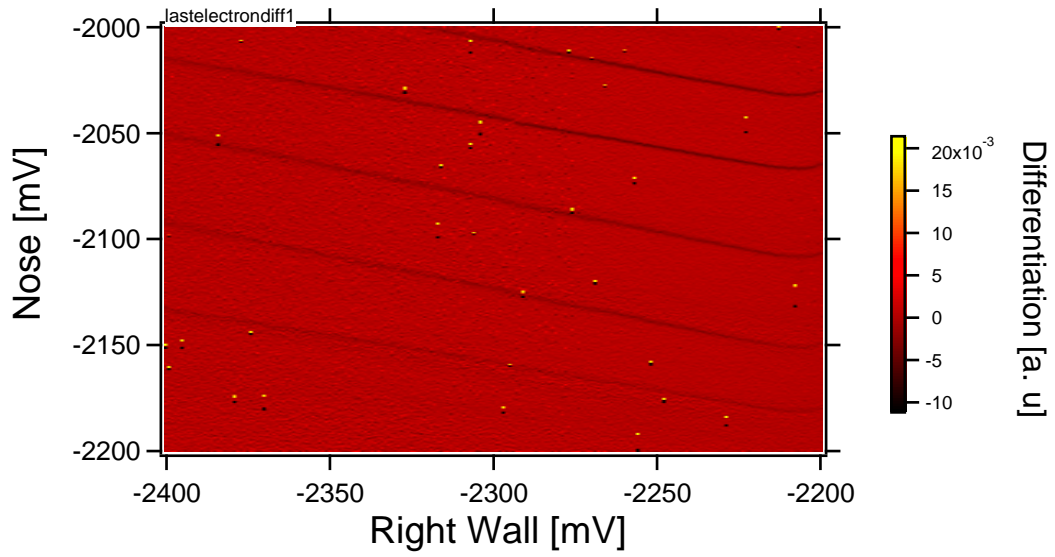


**Figure 4.10.:** Derivative of conductance in respect to the Nose as a function of Nose and Right Wall voltages. Main quantum electron transitions are observable. Gate configuration shown in A.4.

lead to gate leaks. I think it might be, that the vacancies induced by the highly negative gate voltages and the switcher noise might be reducing the resistance from top-gates to the 2DEG and make it easier for gate leaks to happen.

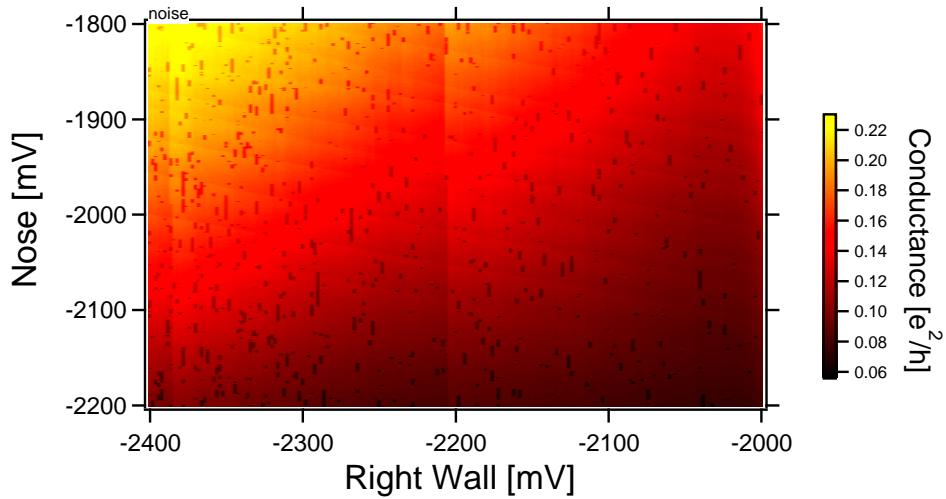


**Figure 4.11.:** Conductance through sensor dot as a function of Nose and Right Wall voltage. Switching noise disturbs the measurement. Gate configuration shown in A.5.

## 5. Conclusion

In this thesis I have investigated a device made of wafer which is specially fabricated for the control of spin-orbit interaction. The wafer properties, especially the low mobility, suggest that measurement are going to be complicated.

Starting with the transport measurements the influence of the low mobility could not be ignored. The formation of a QPC in the 2DEG shows the formation of quantum dot features which we think are deriving from the disorder in the wafer. Transport through the quantum dot solidified the assumption that disorder potential facilitates the formation of undesired quantum dots. In the charge sensing measurement it becomes clear that we form at least six quantum dots instead of one. It has been suggested by S. Wächter in his Master thesis that the influence of the disorder, for a similar wafer (grown by S. Mack, D. Awschalom) increases with more negative BG voltage applied. In addition to the generally low mobility in the wafer the device was taken from edge of the wafer. It has also been shown by S. Wächter that the mobility on the edge of a similar wafer was significantly lower [20]. In addition to the disorder potential disturbing a measurement switching noise is a big problem as TG voltages have been set to be more negative. The switching noise has been studied by M Pioro-Ladriere et al. who has shown that applying positive bias to gates helps in reducing switching noise in GaAs 2DEGs [21].

We were able to tune the quantum dot into a regime where we annihilate the disorder formed dots and form a single quantum dot. We are successfully plunging the quantum dot but could not fully empty the quantum dot because gate leaks prevent further plunging. In respect to the whole project forming single electron quantum dots is crucial. It is possible that for different samples single electron quantum dots can be formed on the wafer used in this thesis. The low mobility is a basic property of the wafer deriving from the growth process. Choosing a sample from a region on the wafer which is more centred might lead to slightly better results, but the maximum mobility is  $\mu = 69'000\text{cm}^2/\text{Vs}$ . In order to make sure that a wafer allowing control of spin-orbit interaction can be used to form quantum dots, a cleaner wafer is required.

## 6. Outlook

In ongoing experiments devices with TG designs as shown in figure 6.1 are fabricated. Two additional TGs positioned above the main quantum dot are introduced. The new TGs together with the BG is supposed to allow to keep the electron density in the quantum dot constant while tuning the strength of the Rashba type spin-orbit interaction. Measuring spin relaxation times then allows to find the regime where  $\alpha = \beta$ , as predicted by I.L. Aleiner et al. and A.V. Khaetskii. [12] [13]. Locally displacing the electron by applying high-frequency pulses to TGs should then allow to perform EDSR.

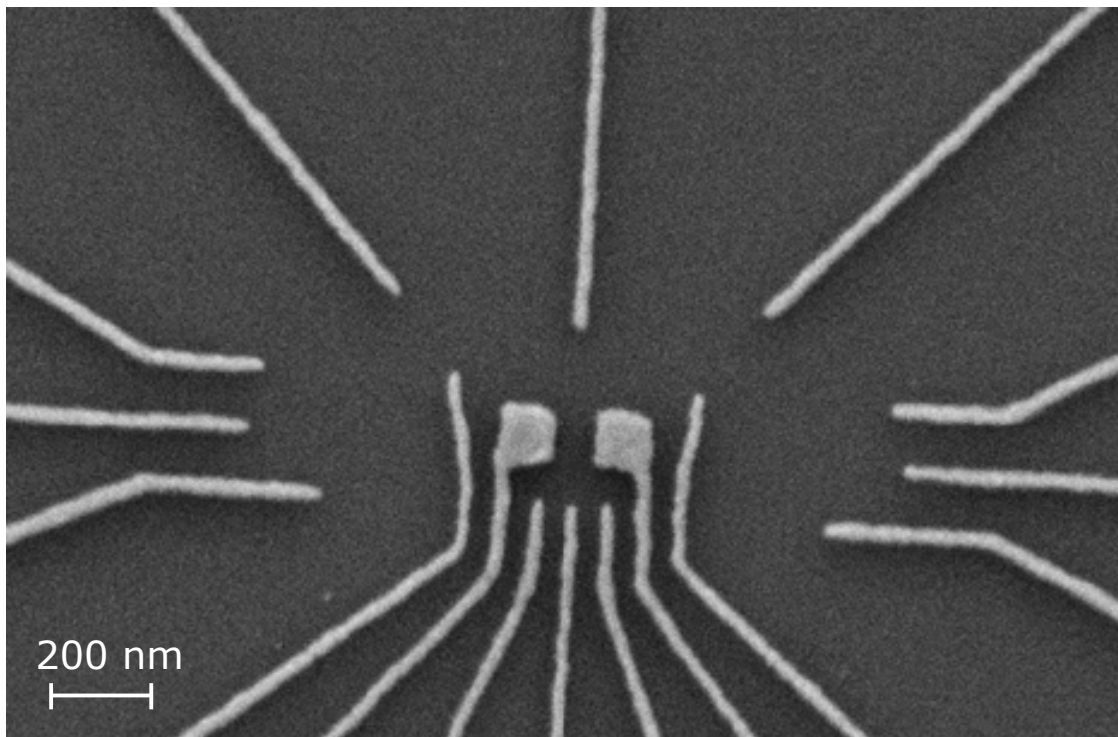


**Figure 6.1.:** New gate design with added large area top gates above the main quantum dot position.

## 7. Acknowledgements

I first of all would like to thank Dominik Zumbühl for giving me the opportunity to do my master thesis in his group. I would like to specially thank Dr. Liuqi Yu and Leon Camenzind for their guidance and many inspiring conversations about quantum dot. I would also like to thank them for the fun off-topic conversations we could have. Special thanks goes to Mirko Rehmann who pointed out to me that Zumbühl group might be the right place for me to write my master thesis. I would like to thank all group members for always being there, may it be for expanding discussions about physics or for just having a good time. Thanks to all of you for contributing to my scientific growth as well as making this thesis a very memorable personal experience. Thanks

# Appendices

## A. Gate Configurations

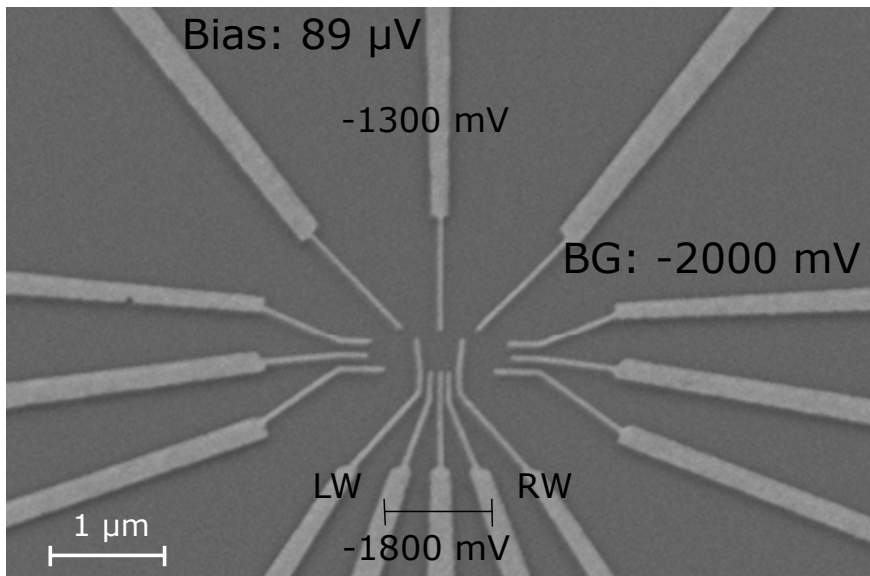


*Figure A.1.*

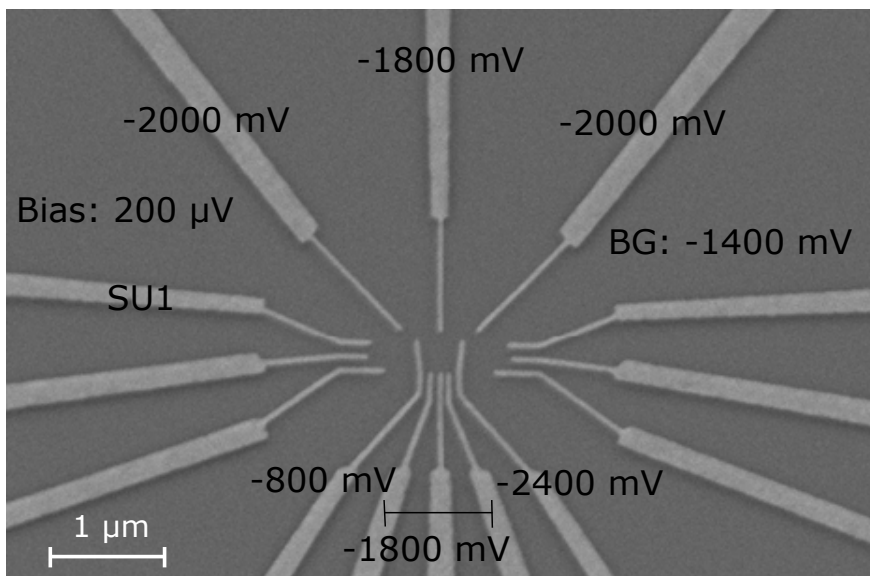


*Figure A.2.*

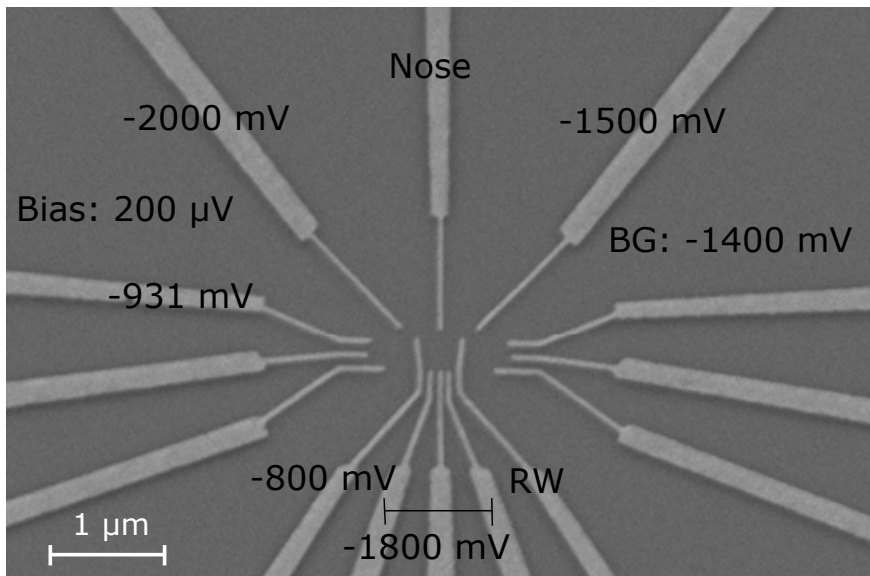


**Figure A.3.**

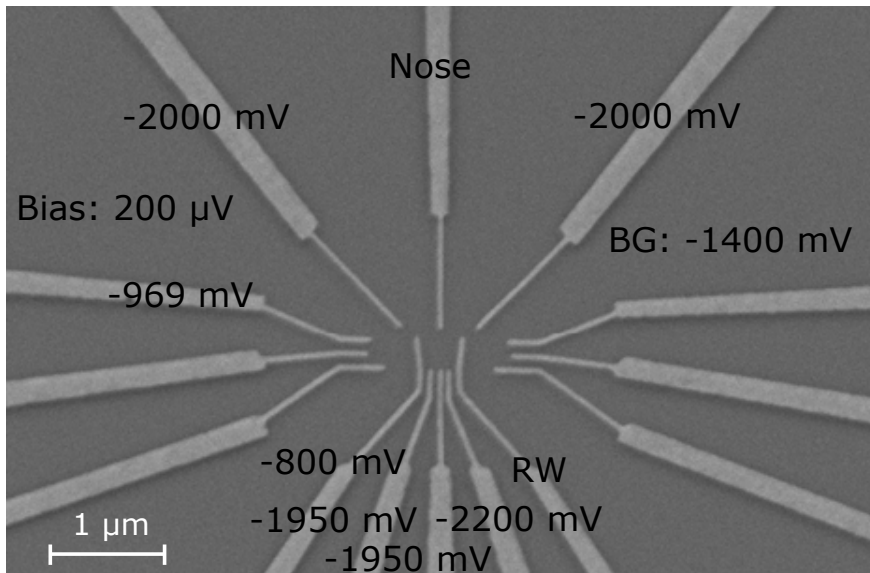


**Figure A.4.**

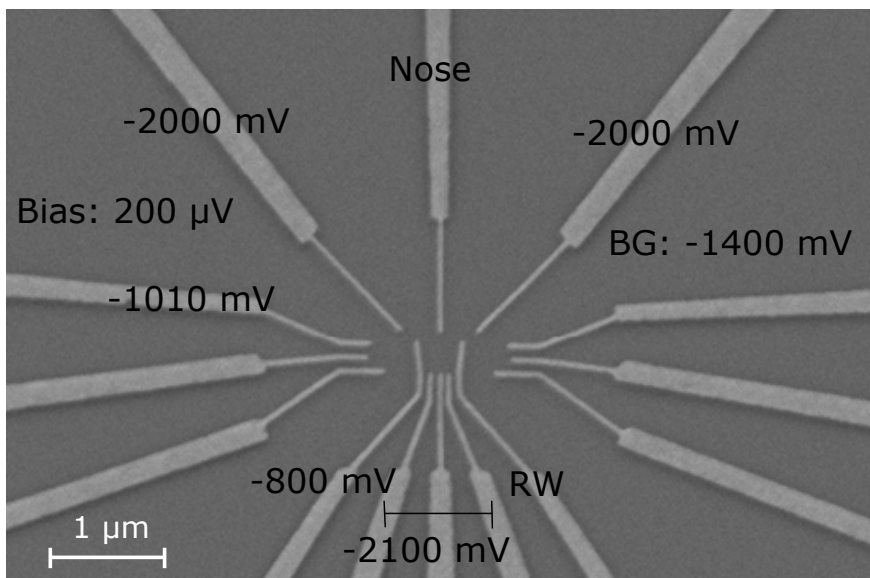


**Figure A.5.**

# Bibliography

- [1] P.W. Shor. Algorithms for quantum computation: discrete logarithms and factoring. *Proceedings 35th Annual Symposium on Foundations of Computer Science*, pages 124–134, 1994.
- [2] Daniel Gottesman. Stabilizer codes and quantum error correction. *arXiv preprint quant-ph/9705052*, 2008:114, 1997.
- [3] D. Jaksch, J. I. Cirac, P. Zoller, R. Côté, and M. D. Lukin. Fast Quantum Gates for Neutral Atoms. *Physical Review Letters*, 85(10):2208–2211, sep 2000.
- [4] J R Weber, W F Koehl, J B Varley, A Janotti, B B Buckley, C G Van de Walle, and D D Awschalom. Quantum computing with defects. *Proceedings of the National Academy of Sciences of the United States of America*, 107(19):8513–8, 2010.
- [5] V Bouchiat, D Vion, P Joyez, D Esteve, and M. H. Devoret. Quantum coherence with a single Cooper pair. *Physica Scripta*, 1998(T76):165, 1998.
- [6] Daniel Loss and David P. DiVincenzo. Quantum computation with quantum dots. *Physical Review A*, 57(1):120–126, jan 1998.
- [7] M. J. Biercuk, S. Garaj, N. Mason, J. M. Chow, and C. M. Marcus. Gate-defined quantum dots on carbon nanotubes. *Nano Letters*, 5(7):1267–1271, 2005.
- [8] Carina Fasth, Andreas Fuhrer, Mikael T. Björk, and Lars Samuelson. Tunable double quantum dots in InAs nanowires defined by local gate electrodes. *Nano Letters*, 5(7):1487–1490, 2005.
- [9] Leo P Kouwenhoven, Charles M Marcus, Paul L McEuen, Seigo Tarucha, Robert M Westervelt, and Ned S Wingreen. *Mesoscopic Electron Trans-*

- port*, chapter Electron Transport in Quantum Dots, pages 105–214. Springer Netherlands, Dordrecht, 1997.
- [10] B. Andrei Bernevig, J. Orenstein, and Shou Cheng Zhang. Exact SU(2) symmetry and persistent spin helix in a spin-orbit coupled system. *Physical Review Letters*, 97(23):1–4, 2006.
  - [11] W. Knap, C. Skierbiszewski, A. Zduniak, E. Litwin-Staszewska, D. Bertho, F. Kobbi, J. L. Robert, G. E. Pikus, F. G. Pikus, S. V. Iordanskii, V. Mosser, K. Zekentes, and Yu. B. Lyanda-Geller. Weak Antilocalization and Spin Precession in Quantum Wells. *Physical Review B*, 53(7):13, 1996.
  - [12] Alexander V Khaetskii and Yuli V Nazarov. Spin relaxation in semiconductor quantum dots. *Physical Review B*, 61(19):12639–12642, 2000.
  - [13] I. L. Aleiner and Vladimir I. Fal’ko. Spin-orbit coupling effects on quantum transport in lateral semiconductor dots. *Physical Review Letters*, 87(25):4, 2001.
  - [14] Thomas Heinzl. *Mesoscopic Electronics in Solid State Nanostructures*. 2003.
  - [15] K. D. Maranowski, J. P. Ibbetson, K. L. Campman, and A. C. Gossard. The conduction barrier at the interface between low temperature grown GaAs and undoped GaAs. *Applied Surface Science*, 104-105(May):621–625, 1996.
  - [16] S Amasha. Electron tunneling and spin relaxation in a lateral quantum dot. *Dissertation*, 2007.
  - [17] M. Stopa. Quantum dot self-consistent electronic structure and the Coulomb blockade. *Physical Review B*, 54(19):13767–13783, 1996.
  - [18] Oliver Bärenbold. *Numerical Simulation of a GaAs Quantum dot*. PhD thesis, 2014.
  - [19] Dominik Zumbhl. *Lecture Notes: Quantum Transport*. 2014.
  - [20] Serge Waechter. *Electric Transport Properties of Quantum Point Contacts in a Gallium Arsenide Quantum Well*. (January), 2014.
  - [21] M. Pioro-Ladrière, John H. Davies, A.R. Long, A.S. Sachrajda, Louis Gau-dreau, P. Zawadzki, J. Lapointe, J. Gupta, Z. Wasilewski, and S. Studenikin.

Origin of switching noise in GaAs/Al<sub>x</sub>Ga<sub>1-x</sub>As lateral gated devices. *Physical Review B*, 72(11):115331, 2005.